

LETTER TO THE EDITOR

Cold and warm molecular gas in the outflow of 4C12.50

K. M. Dasyra¹ and F. Combes¹

Observatoire de Paris, LERMA (CNRS:UMR8112), 61 Av. de l'Observatoire, F-75014, Paris, France

ABSTRACT

We present deep observations of the ^{12}CO (1–0) and (3–2) lines in the ultra-luminous infrared and radio galaxy 4C12.50, carried out with the 30 m telescope of the Institut de Radioastronomie Millimétrique. Our observations reveal the cold molecular gas component of a warm molecular gas outflow that was previously known from *Spitzer* space telescope data. The ^{12}CO (3–2) profile indicates the presence of absorption at -950 km s^{-1} from systemic velocity with a central optical depth of 0.22. Its profile is similar to that of the HI absorption that was seen in radio data of this source. A potential detection of the 0→1 absorption enabled us to place an upper limit of 0.03 on its central optical depth, and to constrain the excitation temperature of the outflowing CO gas to $\geq 65\text{ K}$ assuming that the gas is thermalized. If the molecular clouds fully obscure the background millimeter continuum that is emitted by the radio core, the H_2 column density is $\geq 1.8 \times 10^{22}\text{ cm}^{-2}$. The outflow then carries an estimated cold H_2 mass of at least $4.2 \times 10^3 M_\odot$ along the nuclear line of sight. This mass will be even higher when integrated over several lines of sight, but if it were to exceed $3 \times 10^9 M_\odot$, the outflow would most likely be seen in emission. Since the ambient cold gas reservoir of 4C12.50 is $1.0 \times 10^{10} M_\odot$, the outflowing-to-ambient mass ratio of the warm gas (37%) could be elevated with respect to that of the cold gas.

Key words. ISM: jets and outflows — ISM: kinematics and dynamics — Line: profiles — Galaxies: active — Galaxies: nuclei — Infrared: galaxies

1. Introduction

Through jets, winds, and radiation pressure, active galactic nuclei (AGN) can affect the collapse of their surrounding molecular gas and the formation of new stars in their host galaxies. While simulations attribute a considerable role to AGN feedback in shaping galaxy properties (e.g., Croton et al., 2006; Sijacki et al., 2007; Booth & Schaye, 2009; Hopkins & Elvis, 2010; Debuhr et al., 2012), the question remains open from an observational point of view. Do the AGN-driven outflows that suppress star formation occur frequently enough to affect the observed luminosity and mass functions of galaxies? To answer this question, we not only need to identify objects with massive, AGN-driven outflows of molecular gas, but also to take into account the outflow effects on the different phases of this gas.

The various phases of an AGN-driven molecular gas outflow have been studied in a nearby ultraluminous infrared galaxy (ULIRG), Mrk231. Plateau de Bure interferometric observations showed that the outflowing CO, with a corresponding H_2 mass of $6 \times 10^8 M_\odot$ and a flow rate of $700 M_\odot\text{ yr}^{-1}$, is capable of suppressing star formation (Feruglio et al., 2010). Aalto et al. (2012) discovered the outflow's dense ($\gtrsim 10^4\text{ cm}^{-3}$) component from broad HCN(1–0) profile wings. On the basis of profile fitting of the $79\text{ }\mu\text{m}$ and $199\text{ }\mu\text{m}$ OH lines seen with *Herschel* (Fischer et al., 2010), the outflow contains $\geq 7 \times 10^8 M_\odot$ of molecules. In total, more than $10^9 M_\odot$ of gas can be in the wind.

Another straightforward and quantitative comparison that has yet to be performed is that between the warm and the cold H_2 gas mass in the outflow vs. in the ambient interstellar medium (ISM). A source that is suitable for this analysis is 4C12.50. It is the only source known

to have a massive outflow of gas of few hundred Kelvin, as inferred from its mid-infrared H_2 rotational line profiles (Dasyra & Combes, 2011). In this letter, we present evidence of cold molecules in its outflow, and we evaluate the relative fractions of warm and cold gas that the AGN feedback kinematically distorts. We adopt $H_0=70\text{ km s}^{-1}\text{ Mpc}^{-1}$, $\Omega_M=0.3$, and $\Omega_\Lambda=0.7$ throughout.

2. Data acquisition and reduction

The observations were carried out with the 30 m telescope of the Institut de Radioastronomie Millimétrique on December 21–22 2011, and January 1 2012 (as part of the program 235-11). For the ^{12}CO (1–0) observations, EMIR was tuned to 102.700 GHz. For the ^{12}CO (3–2) observations, the receivers were tuned to 308.086 GHz during the first observing run and to 308.600 GHz during the second observing run, to ensure that the observed line properties were unaffected by possible standing waves, atmospheric line residuals, or bad channels. Parallel to the CO observations, we carried out HCN and HCO^+ (2–1) observations with a common tuning of 158.427 GHz. Both the FTS and WILMA backends, with corresponding resolutions of 0.2 MHz and 2 MHz, were simultaneously used as backends to allow consistency checks. The inner and outer parts of the FTS were used, enabling us to better sample the continuum near each line. The wobbler switching mode with a throw of $80''$ and 0.65 sec per phase was used to rapidly sample the continuum. The telescope pointing accuracy was $2''$, and the system temperature varied from 310 K to 580 K at 1 mm.

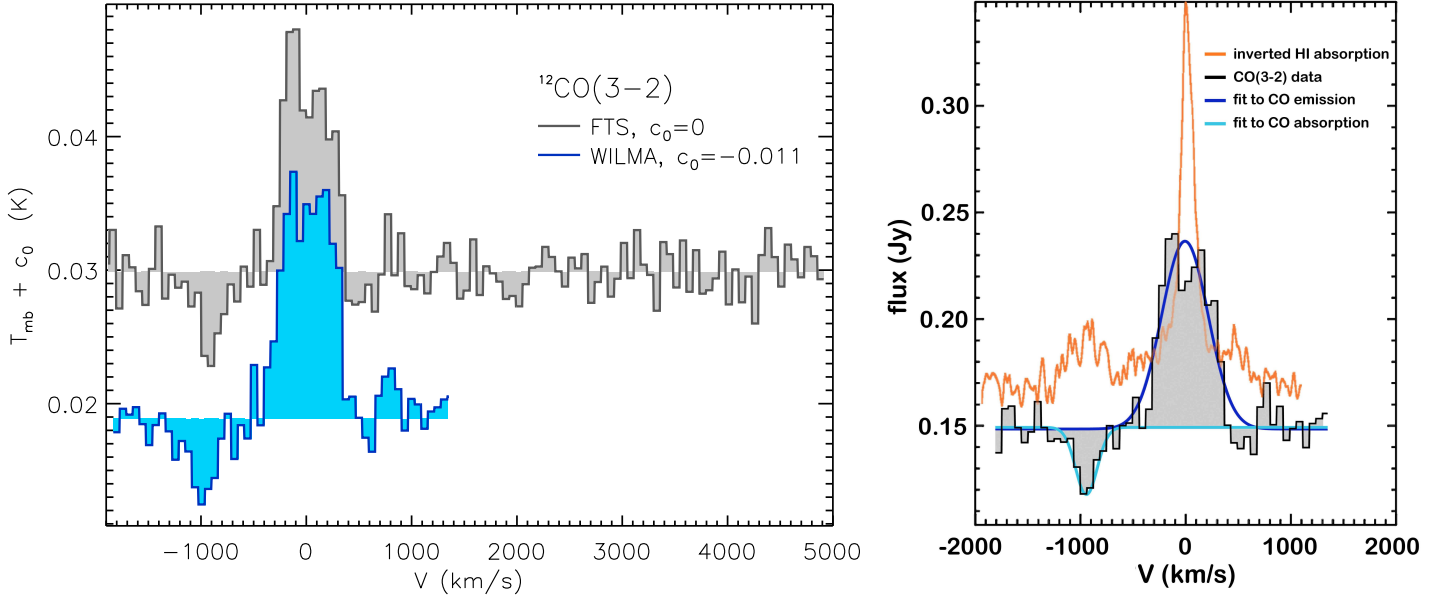


Fig. 1. *Left:* FTS and WILMA spectra of $^{12}\text{CO}(3-2)$ in 4C12.50, binned into 62 km s^{-1} channels and shifted by a constant c_0 , when needed. *Right:* Flux-calibrated line profile of $^{12}\text{CO}(3-2)$, averaged over the WILMA and the FTS data to be least affected by potential artifacts. Gaussian functions with parameters that most closely fit the emission component at the systemic velocity and the absorption component at -950 km s^{-1} are shown in blue and cyan, respectively. The inverse HI absorption that is seen in the radio data of 4C12.50 (Morganti et al., 2004) is overplotted in orange for an arbitrary scale and continuum level.

To reduce the 1 mm data, we removed bad channels from all individual scans. The three parts of each FTS scan, corresponding to the output of a different spectrometer, were fitted with linear baselines and brought to the same continuum level, i.e., to the median value of the full scan. This step was performed to ensure that there is no continuum discontinuity between the three parts that could introduce artificial features into the combined spectrum. We averaged the individual scans of each frequency tuning and backend, discarding scans with unstable baselines. The inner and the outer FTS spectra were then stitched together. For each backend, the spectra of the two frequency tunings were brought to a common reference frequency of 308.245 GHz and averaged. The final spectra are shown in Figure 1. Their total on-source integration time is 2.7 hours.

At 3 mm, we averaged all useful WILMA or FTS scans, after shifting them to a reference frequency of 102.756 GHz and removing bad channels from them. In contrast to the 1 mm data, the 3 mm data had signatures of standing waves owing to the strong synchrotron continuum radiation, which increases with λ . We iteratively fitted the baseline of the WILMA data with sinusoidal functions of periods that are integer multiples of each other, representing different harmonics of the same standing wave. The best-fit solution that was indicated by the CLASS baseline routine corresponded to functions with frequencies of 0.28, 0.84, 1.68, and 2.52 GHz, and an amplitude of 1 mK. These functions were removed from both the WILMA spectrum and the central part of the inner FTS spectrum. The final $^{12}\text{CO}(1-0)$ spectra, with a total on-source integration time of 1.2 hours, are shown in Figure 2. A similar approach was taken for the 2 mm data. A main-beam-temperature-to-flux conversion factor of 5.0 Jy K^{-1} was used to flux calibrate the final spectra at all wavelengths.

3. Results: CO in emission and in absorption

The $^{12}\text{CO}(3-2)$ profile of 4C12.50 consists of an emission component at the galaxy systemic velocity, i.e., at $z=0.1218$, and of an absorption feature at approximately -1000 km s^{-1} from it. The $\text{CO}(2\rightarrow3)$ absorption is seen in all four frequency tuning and backend combinations, indicating that the feature is intrinsic to the source. Its signal-to-noise ratio (S/N) is ~ 6 in both the WILMA and the FTS data, which have a corresponding root-mean-square noise of 1.7 mK and 1.8 mK, respectively. The outer FTS data provide further evidence that the absorption is real by ruling out the existence of standing waves that could create a feature of this depth. The observed optical depth at the center of the line, $\tau_{\text{obs},0}$, is $0.22 (\pm 0.05)$, with an absorption minimum at $30 (\pm 2) \text{ mJy}$ below the local $150 (\pm 20) \text{ mJy}$ continuum. Averaging the best-fit Gaussian parameters of the data for each backend indicates that the minimum is at $-950 (\pm 90) \text{ km s}^{-1}$. The CO absorption profile remarkably resembles that of the HI absorption seen in radio data (Figure 1; Morganti et al., 2004). Its resolution-corrected width is $250 (\pm 80) \text{ km s}^{-1}$, reflecting the collective motions of multiple clouds along the line of sight.

An absorption line is also seen at -1100 km s^{-1} away from $^{12}\text{CO}(1-0)$ after the progressive subtraction of standing wave harmonics from the 3 mm baseline. However, the wave amplitude is comparable to the absorption minimum (Figure 2), impeding its exact profile study. We thus simply constrain $\tau_{\text{obs},0}(0\rightarrow1)$ towards the $0.51 (\pm 0.06) \text{ Jy}$ continuum background to an upper limit of 0.03.

The $^{12}\text{CO}(1-0)$ emission peaks at a main beam temperature of $9.2 (\pm 1.2) \text{ mK}$ above its underlying continuum. Its resolution-corrected width is $400 (\pm 95) \text{ km s}^{-1}$, and its intensity, $I_{\text{CO}(1-0)}$, is $4.0 (\pm 1.3) \text{ K km s}^{-1}$ (see also

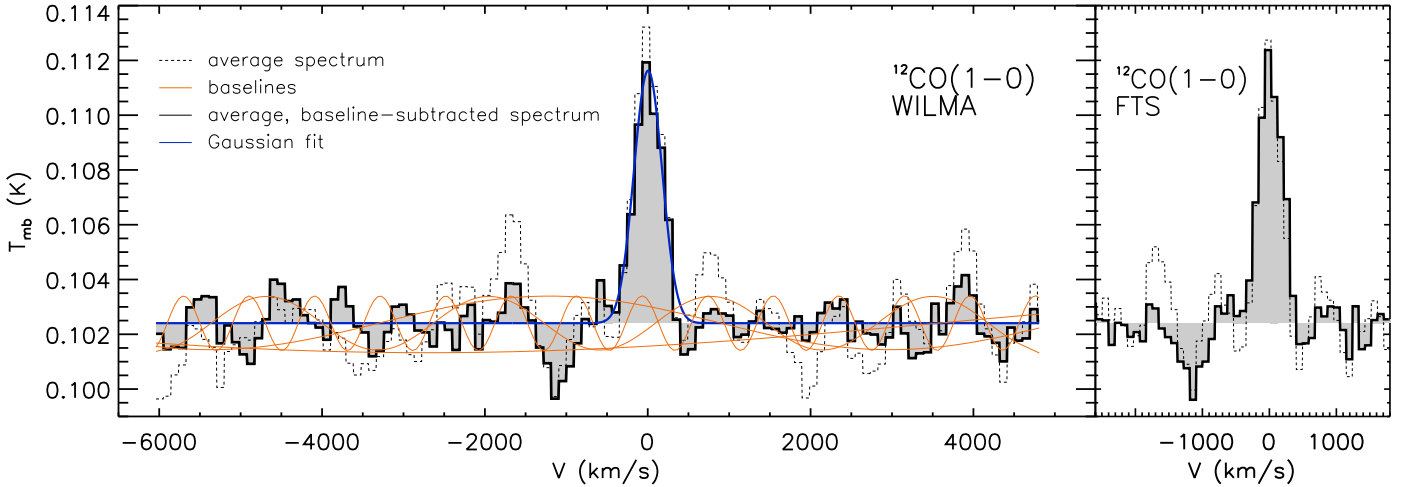


Fig. 2. WILMA (*left*) and FTS (*right*) $^{12}\text{CO}(1-0)$ spectrum of 4C12.50, binned to 93 km s^{-1} channels. The dashed histogram corresponds to the average spectrum prior to the removal of sinusoidal baselines, which represent the harmonics of a standing wave (shown in orange). The final spectrum is shown as a solid, filled histogram.

Evans et al. 1999, 2005). From this, we deduce that the cold H_2 gas reservoir of 4C12.50 is $1.0 (\pm 0.3) \times 10^{10} M_{\odot}$, assuming that the gas mass is given by the product $23.5 \alpha I_{\text{CO}(1-0)} \Omega_B D_L^2 / (1+z)^3 M_{\odot}$ (Solomon et al., 1997), where Ω_B is the telescope main beam area in arcsec², D_L is the source luminosity distance in Mpc, and α is the CO luminosity to H_2 mass conversion factor. We used a 103 GHz beam of $28''$ (61 kpc), and $\alpha = 0.8 M_{\odot} (\text{K km s}^{-1} \text{ pc}^2)^{-1}$ (Downes & Solomon, 1998) because 4C12.50 has a ULIRG-like infrared luminosity ($2.5 \times 10^{12} L_{\odot}$) based on its 12, 25, 60, and $100 \mu\text{m}$ flux (Golombek et al., 1988; Sanders & Mirabel, 1996; Guillard et al., 2012).

The $^{12}\text{CO}(3-2)$ emission is detected with a S/N of 25 and 21 in the WILMA and the FTS data, respectively. Its main beam temperature peaks at $17.5 (\pm 1.0) \text{ mK}$ above the local continuum. Its resolution-corrected width is $510 (\pm 65) \text{ km s}^{-1}$, and its intensity is $9.9 (\pm 1.6) \text{ K km s}^{-1}$.

The $I_{\text{CO}(3-2)} / I_{\text{CO}(1-0)}$ ratio of the ambient gas, 2.5, is below its theoretically predicted value of 9 for the case of optically thick gas that is thermalized to a single T_{ex} . It is also below that of the central line of sight of M82, of several local AGN, ULIRGs, and radio galaxies, but above that of the outflow of M82, and similar to that of the Milky Way. This comparison is visualized in Figure 3 for the line luminosities. Even though this ratio is indicative of large reservoirs of cold and diffuse gas, it does not rule out the presence of a warm and dense, highly excited CO component, which could be detected through high J emission lines. The non-detection of HCN (or HCO^+) at the 3σ level of 0.86 K km s^{-1} for a width of 460 km s^{-1} cannot be used to argue for or against either interpretation. It leads to $I_{\text{CO}} / I_{\text{HCN}} \geq 8$ (Gao & Solomon, 2004) for a linearly interpolated $\text{CO}(2-1)$ intensity of 7 K km s^{-1} .

4. Discussion: on the properties of a multi-phase AGN-driven outflow

The rapid molecular gas motions that we detected provide direct evidence of an outflow in 4C12.50 because none of its merging components (Axon et al., 2000) is moving

faster than $\pm 250 \text{ km s}^{-1}$ from its systemic velocity (Holt et al., 2003; Rodríguez Zaurín et al., 2007). The maximum gas velocity reaches -1500 km s^{-1} , which is atypical of supernova-driven outflows (e.g., Heckman et al., 2000; Rupke et al., 2005), but characteristic of AGN-driven outflows (e.g., Rupke & Veilleux, 2011; Sturm et al., 2011). AGN radiation pressure and winds can affect the gas kinematics in 4C12.50: the AGN radiation does reach and ionize part of the outflowing gas, which contains both Ne V and O IV ions (Spoon & Holt, 2009; Dasyra et al., 2011). The gas can also be pushed by shocks created as the radio jet of 4C12.50 (Stanghellini et al., 1997) propagated through the ISM. An HI outflow in front of a bright radio knot (Morganti et al., 2004) makes this scenario plausible for the neutral gas, and even for the molecular gas. A jet-ISM interaction can be responsible for the irregular H_2 kinematics (Dasyra & Combes, 2011; Nesvadba et al., 2011), the strong H_2 emission (Ogle et al., 2010), and the high CO excitation (Papadopoulos et al., 2008) of radio galaxies.

To constrain the line-of-sight CO column density, N_{CO} , from the observed absorption, we assume that the gas is homogeneously distributed and in local thermodynamic equilibrium (LTE). We can then relate N_{CO} to τ through

$$N_{\text{CO}} = 8\pi \frac{\nu^3}{c^3} \frac{Q(T_{\text{ex}}) e^{E_J/kT_{\text{ex}}}}{g_{J+1} A_{J+1,J} (1 - e^{-h\nu/kT_{\text{ex}}})} \int \tau dV \quad (1)$$

(e.g., Wiklind & Combes, 1995), where c is the lightspeed, h is the Planck constant, k is the Boltzmann constant, E_J and g_J are the energy and the statistical weight of the state J , respectively, $A_{J+1,J}$ is the Einstein coefficient for spontaneous emission, ν is the frequency of the emitted line, and Q is the partition function at the excitation temperature T_{ex} . The ratio $\int \tau(2 \rightarrow 3) dV / \int \tau(0 \rightarrow 1) dV$ agrees with its observed limit, > 6.4 , if $T_{\text{ex}} \geq 65 \text{ K}$. Turbulence and shocks can easily bring the gas to this T_{ex} through collisions. For $T_{\text{ex}} = 65 \text{ K}$, N_{CO} is equal to $1.8 \times 10^{18} \text{ cm}^{-2}$.

This number will increase with increasing T_{ex} , but will remain on the same order of magnitude up to 200 K. The filling factor of the background source by the molecular clouds, f_c , can play an important role in the T_{ex} and

N_{CO} determinations. Partial coverage of the background source ($f_c < 1$) can cause the observed (beam-averaged) optical depth to deviate from its actual value, which is then equal to $-\ln[1 - (1 - e^{-\tau_{\text{obs}}})/f_c]$ (Wiklind & Combes, 1994). For gas in LTE, this relation is computed from the radiative transfer equation, assuming that $T_{\text{ex}} \ll T_{\text{bg}}$ and that the cosmic microwave background contribution to the gas excitation is negligible (e.g., Staguhn et al., 1997). Requiring the gas to be optically thick limits f_c to values above 0.2. Data of multiple transitions are needed to measure f_c , further constrain N_{CO} , and examine any large velocity gradients (Scoville & Solomon, 1974) and different energy level populations (Israel et al., 1991).

For the present assumptions and a CO-to- H_2 abundance ratio of 10^{-4} , the H_2 column density towards the outflow, N_{H_2} , is $\gtrsim 2 \times 10^{22} \text{ cm}^{-2}$. The HI column density is $3 \times 10^{21} \text{ cm}^{-2}$, based on both optical NaI data (Rupke et al., 2005) and radio HI data (Morganti et al., 2005, for $T_{\text{spin}} = 1000 \text{ K}$). For the ambient HI gas, which is located 100 pc northwest of the radio core, the column density is $6 \times 10^{20} \text{ cm}^{-2} - 10^{22} \text{ cm}^{-2}$ (Morganti et al., 2004; Curran & Whiting, 2010, for $T_{\text{spin}} = 100 \text{ K}$). The largest uncertainty in this comparison is the wavelength-dependent spatial distribution of the background and the foreground source. The radio core emission typically dominates the millimeter and even the submillimeter ($850 \mu\text{m}$; Clements et al. 2010) continuum, because the emission from diffuse jet knots is described by a steep power law that declines rapidly with frequency (Krichbaum et al., 1998, 2008). We thus assume that the millimeter background source area is contained within the 2 cm beam.

For a beam area of 3 milliarcsec² (Lister et al., 2003) and $N_{\text{H}_2} = 1.8 \times 10^{22} \text{ cm}^{-2}$, the outflow entrains $4.2 \times 10^3 M_{\odot}$ of cold H_2 gas in front of the millimeter core. How this mass compares with the mass of the cold H_2 gas that flows over all lines of sight is unknown. It therefore remains unclear whether the outflow carries less cold than warm H_2 gas. However, the outflowing-to-ambient mass ratio of the cold gas will be lower than that of the 400 K gas (37%; Dasyra & Combes 2011), as long as the cold outflowing gas weighs less than $3 \times 10^9 M_{\odot}$. If this amount of gas existed in the millimeter beam, and without a background source illuminating most of the clouds, the outflow would be seen in emission. Our $^{12}\text{CO}(0 \rightarrow 1)$ data instead limit any additional outflowing cold gas mass to be $\leq 2 \times 10^9 M_{\odot}$ when integrating over a 1000 kpc² area and a 1500 km s^{-1} velocity range (Batcheldor et al., 2007).

5. Summary

We have presented deep 30 m observations of $^{12}\text{CO}(1-0)$ and $(3-2)$ in the nearby ULIRG and radio galaxy 4C12.50, which has an impressive outflow of warm (400 K) H_2 gas (Dasyra & Combes, 2011). Our observations led to the discovery of the cold component of the molecular outflow. Absorption from $J=2 \rightarrow 3$ is seen in data obtained with two different frequency tunings and backends. It peaks at -950 km s^{-1} , and its profile resembles that of the HI absorption component that traces the neutral gas outflow (Morganti et al., 2004). Absorption is also potentially seen for the $0 \rightarrow 1$ transition. Treating the optical depth of the latter as an upper limit and assuming that the clouds fully cover their background source, we have found that

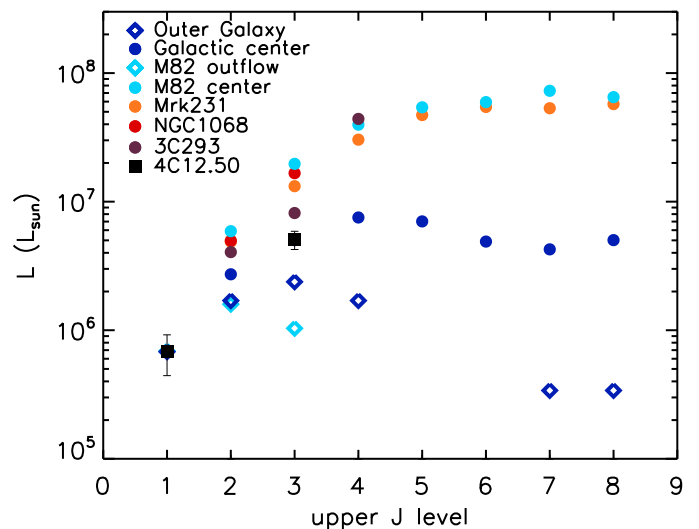


Fig. 3. CO line luminosities in 4C12.50 and other sources, normalized to $L_{\text{CO}(1-0)}(4\text{C12.50})/L_{\text{CO}(1-0)}$. The data are from Fixsen et al. (1999), Dumke et al. (2001), Weiss et al. (2001, 2005), Papadopoulos et al. (2007, 2008), Panuzzo et al. (2010), van der Werf et al. (2010), and Krips et al. (2011). Typical uncertainties are 0.1-0.3 dex.

the molecular gas has an excitation temperature of at least 65 K in LTE conditions. For this temperature, N_{H_2} is $1.8 \times 10^{22} \text{ cm}^{-2}$. This suggests that the outflow carries $4.2 \times 10^3 M_{\odot}$ of cold H_2 gas along the nuclear line of sight. Even if the mass of the cold outflowing gas could exceed that of the warm outflowing gas, $5.2 \times 10^7 M_{\odot}$, for a higher N_{CO} value or when integrating over several lines of sight, it would most likely not exceed $3 \times 10^9 M_{\odot}$, i.e., one third of the ambient cold gas reservoir. The outflowing-to-ambient mass ratio could thus be elevated into the warm gas phase with respect to the cold gas phase.

Acknowledgements. K. D. acknowledges support by the Centre National d'Etudes Spatiales (CNES), and is thankful to P. Salomé for technical tips and to P. Papadopoulos for useful discussions. Based on data obtained with the 30 m telescope of IRAM, which is supported by INSU/CNRS (France), MPG (Germany), and IGN (Spain).

References

- Aalto, S., Garcia-Burillo, S., Muller, S., et al. 2012, *A&A*, 537, 44
- Axon, D. J., Capetti, A., Fanti, R., et al. 2000, *AJ*, 120, 2284
- Batcheldor, D., Tadhunter, C., Holt, J., et al. 2007, *ApJ*, 661, 70
- Booth, C. M., & Schaye, J. 2009, *MNRAS*, 398, 53
- Clements, D. L., Dunne, L., & Eales, S. 2010, *MNRAS*, 403, 274
- Croton, D. J., Springel, V., White, S. D. M., et al., 2006, *MNRAS*, 367, 864
- Curran, S. J., & Whiting, M. T. 2010, *ApJ*, 712, 303
- Dasyra, K. M., Ho, L. C., Netzer, H., et al. 2011, *ApJ*, 740, 94
- Dasyra, K. M., & Combes, F. 2011, *A&A*, 533, L10
- Debuhr, J., Quataert, E., & Ma, C.-P. 2012, *MNRAS*.tmp.2150
- Downes, D., & Solomon, P. M. 1998, *ApJ*, 507, 615
- Dumke, M., Nietten, C., Thuma, G., et al. 2001, *A&A*, 373, 853
- Evans, A. S., Mazzarella, J. M., Surace, J., et al. 2005, *ApJS*, 159, 197
- Evans, A. S., Kim, D. C., Mazzarella, J. M., et al. 1999, *ApJ*, 521, L107
- Feruglio, C., Maiolino, R., Piconcelli, E., et al. 2010, *A&A*, 518, L155
- Fischer, J., Sturm, E., González-Alfonso, E., et al. 2010, *A&A*, 518, L41
- Fixsen, D. J., Bennett, C. L., & Mather, J. C. 1999, *ApJ*, 526, 207
- Gao, Yu, & Solomon, P. M. 2004, *ApJ*, 606, 271
- Golombek, D., Miley, G. K., & Neugebauer, G. 1988, *AJ*, 95, 26

- Guillard, P., Ogle, P., Emonts, B., et al. 2012, *ApJ*, 747, 95
- Heckman, T. M., Lehnert, M. D., Strickland, D. K., & Armus, L. 2000, *ApJS*, 129, 493
- Holt, J., Tadhunter, C. N., & Morganti, R. 2003, *MNRAS*, 342, 227
- Hopkins, P. F., & Elvis, M. 2010, *MNRAS*, 401, 7
- Israel, F. P., van Dishoeck, E., Baas, F., et al. 1991, *A&A*, 245, L13
- Krichbaum, T. P., Alef, W., Witzel, A., et al., 1998, *A&A* 329, 873
- Krichbaum, T. P., Lee, S. S., Lobanov, A. P., et al. 2008, *ASPC*, 386, 186
- Krips, M., Martn, S., Eckart, A., et al. 2011, *ApJ*, 736, 37
- Lister, M. L., Kellermann, K. I., Vermeulen, R. C., et al. 2003, *ApJ*, L584, 135
- Morganti, R., Oosterloo, T. A., Tadhunter, C. N., et al. 2004, *A&A*, 424, 119
- Morganti, R., Tadhunter, C. N., & Oosterloo, T. A. 2005, *A&A*, 444, L9
- Nesvadba, N., Boulanger, F., Lehnert, M., et al. 2011 *A&A*, 536, L5
- Ogle, P., Boulanger, F., Guillard, P., 2010, *ApJ*, 724, 1193
- Panuzzo, P., Rangwala, N., Rykala, A., et al. 2010, *A&A*, 518, L37
- Papadopoulos, P. P., Isaak, K. G., & van der Werf, P. P. 2007. *ApJ*, 668, 815
- Papadopoulos, P. P., Kovacs, A., Evans, A. S., & Barthel, P. 2008, *A&A*, 491, 483
- Rodríguez Zaurín, J., Holt, J., Tadhunter, C. N., & González Delgado, R. M. 2007, *MNRAS*, 375, 1133
- Rupke, D. S., Veilleux, S., & Sanders, D. B. 2005, *ApJ*, 632, 751
- Rupke, D. S. N., & Veilleux, S. 2011, *ApJ*, 729, L27
- Sanders, D. B., & Mirabel, I. F. 1996, *ARA&A*, 34, 749
- Sijacki, D., Springel, V., Di Matteo, T., & Hernquist, L. 2007, *MNRAS*, 380, 877
- Scoville, N. Z., & Solomon, P. M. 1974, *ApJ*, 187, L67
- Solomon, P. M., Downes, D., Radford, S. J. E., & Barrett, J. W. 1997, *ApJ*, 478, 144
- Spoon, H. W. W., & Holt, J. 2009, *ApJ*, 702, L42
- Staguhn, J., Stutzki, J., Chamberlin, R. A., et al. 1997, *ApJ*, 491, 191
- Stanghellini, C., O’Dea, C. P., Baum, S. A., et al. 1997 *A&A*, 325, 943
- Sturm, E., González-Alfonso, E., Veilleux, S., et al. 2011, *ApJ*, 733, L16
- van der Werf, P. P., Isaak, K. G., Meijerink, R., et al. 2010, *A&A*, L518, 42
- Weiss, A., Neininger, N., Hüttemeister, S., & Klein, U. 2001, *A&A*, 365, 571
- Weiss, A., Walter, F., & Scoville, N. Z. 2005, *A&A*, 438, 533
- Wiklind, T. & Combes, F. 1994, *A&A*, 286, L9
- Wiklind, T. & Combes, F. 1995, *A&A*, 299, 382